Disorder-order phase transition at high pressure in ammonium fluoride

Christophe Bellin,[1,*] Adrien Mafety,[1] Chandrabhas Narayana,[2] Paola Giura,[1] Gwenaelle Rousse,[3] Jean-Paul Itié,[4] Alain Polian,[1] A. Marco Saitta,[1] and Abhay Shukla[1,†]

[1]*Institut de Minéralogie, de Physique des Matériaux et de Cosmochimie, Sorbonne Universités–Université Pierre et Marie Curie Paris 6, CNRS UMR 7590, IRD UMR 206, Museum national d'Histoire naturelle, F-75005 Paris, France*

[2]*Chemistry and Physics of Materials Unit, Jawaharlal Nehru Centre for Advanced Scientific Research, Jakkur, Bangalore 560064, India*

[3]*UMR8260 "Chimie du Solide et Energie", Collège de France, 11 place Marcelin Berthelot, 75231 Paris Cedex 05, France and Sorbonne Universités–UPMC University Paris 06, 4 Place Jussieu, 75005 Paris, France*

[4]*Synchrotron SOLEIL, Boîte Postale 48, 91192 Gif sur Yvette, France*

(Received 23 March 2017; revised manuscript received 3 July 2017; published 25 September 2017)

Solid NH_4F displays intriguing parallels with ice despite its apparently ionic character. Here we investigate its phase diagram in low-temperature and high-pressure regions using Raman spectroscopy, x-ray diffraction, and *ab initio* structure search calculations. We focus on the high-pressure cubic phase which resembles that found in ice under pressure and is also the ambient pressure phase of other ammonium halides. We detect a disorder-order transition above 10 GPa, recalling those found both in other ammonium halides and in ice. The transition reveals itself in the pressure dependence of several Raman modes as well as through the progressive splitting of lattice and bending modes of the cubic phase at low temperatures. An in-depth analysis of the Raman modes and their evolution is made.

DOI: 10.1103/PhysRevB.96.094110

I. INTRODUCTION

Ammonium salts are generally considered to be ionic systems due to the similarity of their properties and structures (NaCl or CsCl type) with potassium, rubidium, and cesium salts, and due to the similarity of the sizes of the cations. Ammonium fluoride (NH_4F), however, is different, being isostructural to ice Ih in ambient conditions, with local tetrahedral coordination and hydrogen bonding [1–3]. As in ice, the hexagonal phase transits to rhombohedral and cubic phases with the increase of pressure, as shown in the schematic phase diagram in Fig. 1. Earlier work has mainly used x-ray and neutron diffraction and Raman spectroscopy in the 0–16 GPa range to establish the low-pressure room-temperature phase diagram of NH_4F. At ambient temperature, the room-pressure hexagonal phase NH_4F I [4,5] transits at about 0.36 GPa to the rhombohedral phase NH_4F II [6,7]. At higher temperature, a small region beyond 400 K and below 1 GPa is characterized by a NaCl-type cubic phase (NH_4F IV), while at still higher temperatures and in the same pressure range, the liquid phase is reported [8,9]. At pressure higher than 1 GPa, a CsCl-type cubic phase (NH_4F III [6]) similar to the other halides, is found to be stable to the highest pressures measured of about 16 GPa [10].

NH_4F I is a wurtzite-type structure with space group $P6_3mc$ compared to ice Ih with space group $P6_3/mmc$, while NH_4F II belongs to the space group $R3c$ [11] compared to ice II with space group $R\bar{3}$ [12]. A key feature of the ice phase diagram is an order-disorder transition between the ice-VII and ice-VIII phases. Above 1 GPa, cubic ice VII consists of two interpenetrating cubic lattices just as in cubic NH_4F III. Ice VII is disordered with respect to proton positions with the ice rules satisfied locally [13]. It undergoes a small tetragonal distortion to ice VIII [14] below 278 K. This compression along the c axis of the new structure is driven by hydrogen ordering. The other ammonium halides, which are cubic in ambient conditions, are also known to undergo temperature- and pressure-dependent order-disorder transitions [15,16] related to the hydrogen bond. These analogies between NH_4F and ice, on the one hand, and the other ammonium halides, on the other, bring up important and as yet unanswered questions. Is NH_4F III a disordered phase and does an ordering transition exist? Does the behavior of NH_4F resemble that of ice or that of the other halides? In the following, we answer these questions with Raman scattering and x-ray diffraction measurements as a function of pressure and/or temperature as well as an *ab initio* computational structure search. We find consistent results indicating that NH_4F III is a disordered phase in ambient conditions which orders at high pressure. At low temperature, this ordered phase exhibits a tetragonal distortion. This transition has similarities with both the behavior found in ice and in other ammonium halides.

II. HIGH-PRESSURE X-RAY DIFFRACTION

Ammonium fluoride purchased from Aldrich (99.99%) was loaded with neon as the transmitting medium and a stainless steel gasket with a hole of 200 μm in a diamond-anvil cell of 400 μm culet diameter. Pressure was monitored with the emission line of a ruby [17]. X-ray diffraction was performed at the PSICHE beam line (SOLEIL Synchrotron), using 0.3738 Å wavelength radiation. Diffractograms were recorded for pressures from 5 to 26 GPa and at 292 K on a two-dimensional (2D) MarCCD detector and integrated with the FIT2D program [18] to get conventional powder-diffraction patterns. These were fitted using the Rietveld method [19] as implemented in the FULLPROF suite of programs [20] with the lattice parameter, background, line shape (using a Thompson-Cox-Hastings pseudo-Voigt function), and angular shift to account for possible misalignments as parameters.

*christophe.bellin@upmc.fr
†abhay.shukla@upmc.fr

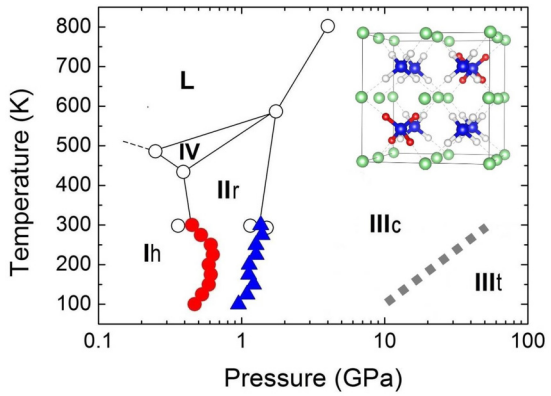

FIG. 1. A schematic phase diagram of the three known ambient and high-pressure phases of ammonium fluoride including the phase transition from the cubic (IIIc) to the tetragonal (IIIt) phase found in this work. Empty circles and straight lines are from previous work. Filled circles and triangles which define phase boundaries between the three phases are measured data from this work. Pressure was increased while cycling between low and ambient temperature.

Atomic positions of N and F were fixed because they are at special Wyckoff positions of space group $P\bar{4}3m$ [F at (0,0,0) and N at (0.5,0.5,0.5)]. H positions, not detected by x rays, were not included in the refinement.

We focus on the high-pressure cubic structure of NH_4F III with the $P\bar{4}3m$ space group and containing 1 formula unit (f.u.) per unit cell NH_4F [6]. In the $P\bar{4}3m$ cell, nitrogen atoms are located on the center (1*b* sites), fluorine at the corners (1*a* site), and hydrogen atoms around the nitrogen atoms in a tetrahedral configuration, as shown in Fig. 2(a).

Some integrated diffraction spectra at various pressures are shown in Fig. 3(c), while 2D as-measured diffractograms for these spectra are shown in Fig. 4. Examples of Rietveld refinement performed at 6 and 25.5 GPa are shown in Figs. 3(a) and 3(b). The symbols in Fig. 3(d) show the variation of the cubic lattice parameter a as a function of pressure at 292 K. The parametrized equation of state [21] is calculated for pressure points below 20 GPa with a satisfactory fit and yields

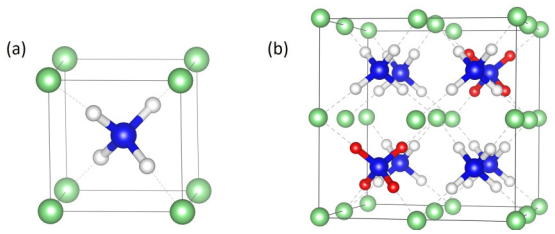

FIG. 2. (a) The $P\bar{4}3m$ structure: small spheres (gray) represent hydrogen, the central sphere (blue) represents nitrogen, and corner spheres (green) represent fluorine. The solid lines depict the unit cell and the dashed lines indicate the hydrogen bonds. N-H bonds are along $[11\bar{1}]$, $[\bar{1}\bar{1}\bar{1}]$, $[\bar{1}11]$, and $[1\bar{1}1]$ directions. (b) The $2 \times 2 \times 2$ supercell model: six ammonium ions (white spheres for hydrogen) are in the tetrahedral configuration (N-H bonds along the $[11\bar{1}]$, $[\bar{1}\bar{1}\bar{1}]$, $[\bar{1}11]$, and $[1\bar{1}1]$ directions), while two ammonium ions (red spheres for hydrogen) are in the antitetrahedral configuration ([111], $[1\bar{1}\bar{1}]$, $[\bar{1}1\bar{1}]$, and $[\bar{1}\bar{1}1]$ directions).

a bulk modulus of 33.9 ± 0.9 GPa (with $B' = 4.1 \pm 0.2$ GPa). For pressure exceeding 20 GPa, there is a deviation from the expected behavior as indicated by the flattening of the experimental equation of state, a point that will be discussed below. X-ray powder-diffraction results are limited by the tendency of NH_4F to crystallize in large-size grains under pressure whether the precursor in the high-pressure cell is a single crystal or powder (Fig. 4).

The (P,V) phase diagram was modeled using the *ab initio* random structure searching (AIRSS) method [22] in order to predict the most promising crystalline phases at given pressures. These *ab initio* structural searches generate and optimize random structures to a minimum in the enthalpy using density functional theory (DFT). We carried out searches at different fixed pressures: 0, 9, 13, and 30 GPa, using 1, 2, 3, 4, and 5 f.u. of NH_4F per unit cell. At 0 GPa, the lowest predicted enthalpy structure is the NH_4F I phase. At 9, 13, and 30 GPa, we always found the lowest enthalpy structure to be the $P\bar{4}3m$ space group also found in experiment (see Supplemental Material [23]).

The experimental equation of state is compared to the calculated ones for the $P\bar{4}3m$ structure in Fig. 3(d). We carried out structural relaxations at fixed pressure in order to calculate the equation of state of the $P\bar{4}3m$ structure and the $2 \times 2 \times 2$ supercell. Geometry optimization calculations (DFT) were performed with the PW code of the QUANTUM ESPRESSO [28] package within different generalized gradient approximations (GGAs) such as the Perdew-Burke-Ernzerhof (PBE) [29] and PBEsol [30] exchange-correlation functionals and a plane-wave basis set. Monkhorst-Pack (MP) **k**-point grids typically containing 4–28 points were used for the Brillouin zone sampling with an energy cutoff of 1090 eV. Convergence was assumed when the energy changed by less than 10^{-7} eV between self-consistent field steps. In Fig. 3(d), we show the variation of the cubic cell parameter normalized to the 0 GPa values. The theoretical bulk moduli (47.2 GPa with $B' = 4.3 \pm 0.2$ GPa for PBE and 56.3 GPa with $B' = 4.5 \pm 0.2$ GPa for PBEsol) are overestimates of experiment (33.9 GPa), while the 0 GPa lattice parameter is underestimated.

The primitive unit cell of the $P\bar{4}3m$ structure shown in Fig. 2(a) presupposes a perfectly ordered crystal, which is improbable at nonzero temperatures. Indeed, all the other halides in the cubic CsCl structure are disordered at high temperature, in the so-called phase II [31–34]. A change in the orientation of the central tetrahedron involves the breaking and reforming of H bonds and the rotation of the central NH_4^+ ion only, since the corner F^- ions are strictly identical. The tetrahedra thus assume one of two positions in a disordered way at high temperature. As the statistically meaningful *ab initio* calculations of large-scale disordered structures are computationally out of reach, we simulate disorder (or lower symmetry) by adopting a $2 \times 2 \times 2$ supercell, shown in Fig. 2(b), containing six NH_4^+ ions in the tetrahedral configuration and two NH_4^+ ions in the (other) antitetrahedral configuration with N-H bonds oriented in [111], $[1\bar{1}\bar{1}]$, $[\bar{1}1\bar{1}]$, and $[\bar{1}\bar{1}1]$ directions. The N atoms of these two NH_4^+ ions are, respectively, located at the (0.25,0.25,0.25) and (0.75,0.75,0.75) positions. The choice of this supercell was reached after considering two other simple possibilities, including one antitetrahedral and four antitetrahedral cells per

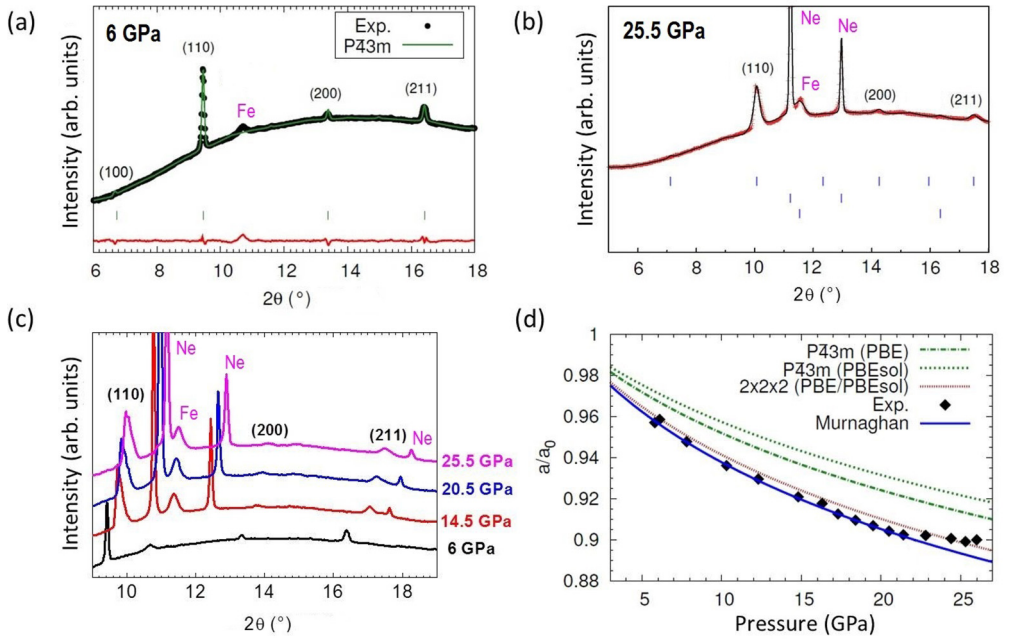

FIG. 3. (a),(b) Rietveld refinement of cubic NH_4F III at 6 and 25.5 GPa and at 292 K. Black dots: experimental spectrum; green line: calculated pattern; lower line (red): observed-calculated difference. Vertical tick marks are the Bragg reflections in the $P\bar{4}3m$ space group. (c) Integrated spectra at various pressures showing contributions from the sample, from solid Ne (except at 6 GPa) and from the gasket (G). (d) Calculated a/a_0 ratio with experimental data (diamonds) and the parametrized fit (solid line) as a function of pressure. The experimental error bars are smaller than the symbols. The data deviate from the fit above 20 GPa. Pressure and volume are calculated using DFT with the PBE and PBEsol functionals for the exchange correlation. The values of a_0 used for the $P\bar{4}3m$ structure are 3.31 Å (PBE) and 3.24 Å (PBEsol). The values of a_0 (per f.u.) for the $2 \times 2 \times 2$ supercell are 3.37 Å (PBE), 3.33 Å (PBEsol), and 3.35 Å (experiment).

$2 \times 2 \times 2$ supercell. These latter possibilities, which are more "ordered," consequently underestimate the lattice parameter and overestimate the bulk modulus. The calculated bulk moduli (36.6 GPa with $B' = 4.3 \pm 0.2$ GPa for PBE and 35.2 GPa with $B' = 4.4 \pm 0.2$ GPa for PBEsol) for the $2 \times 2 \times 2$ supercell with two antitetrahedral unit cells are in much better agreement with the experimental value (33.9 GPa), implying disorder of the NH_4^+ tetrahedron in the extended crystal structure at high temperature. We have thus explained this fact, known in the other ammonium halides, using our experimental equation of state and a simple simulated model for disorder. We now come back to the flattening of the experimental equation of state at about 20 GPa which causes it to deviate from the calculation for the model disordered supercell. The direction of

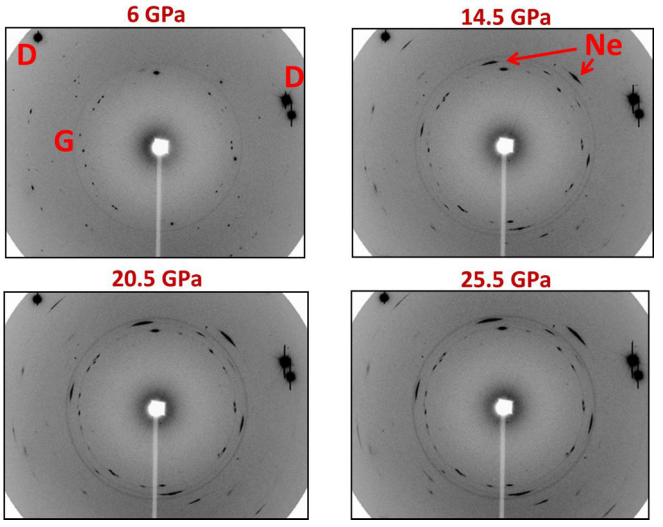

FIG. 4. As-measured 2D diffractograms at various pressures showing contributions from the few crystalline grain sample, with intense spots from diamond anvils (D) and rings from the gasket (G) and from solid neon.

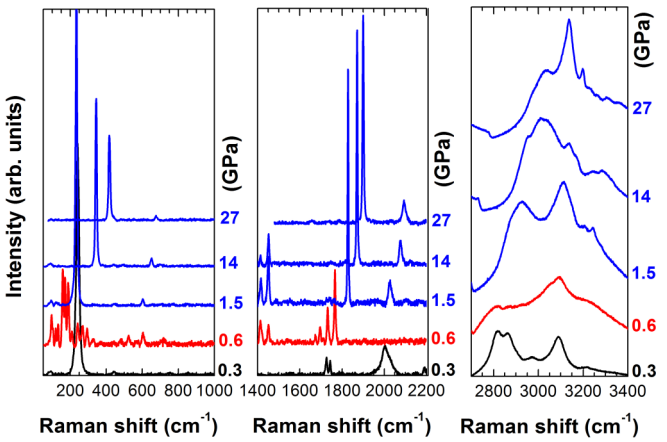

FIG. 5. Variation of experimental Raman spectra at 295 K for a few chosen pressures showing the principal phases. From left to right: lattice and librational modes, NH_4^+ bending region, and N-H stretching region. Hexagonal NH_4F I spectrum at 0.3 GPa (black); rhombohedral NH_4F II spectrum at 0.6 GPa (red); cubic NH_4F III spectra at 1.5 GPa and above (blue).

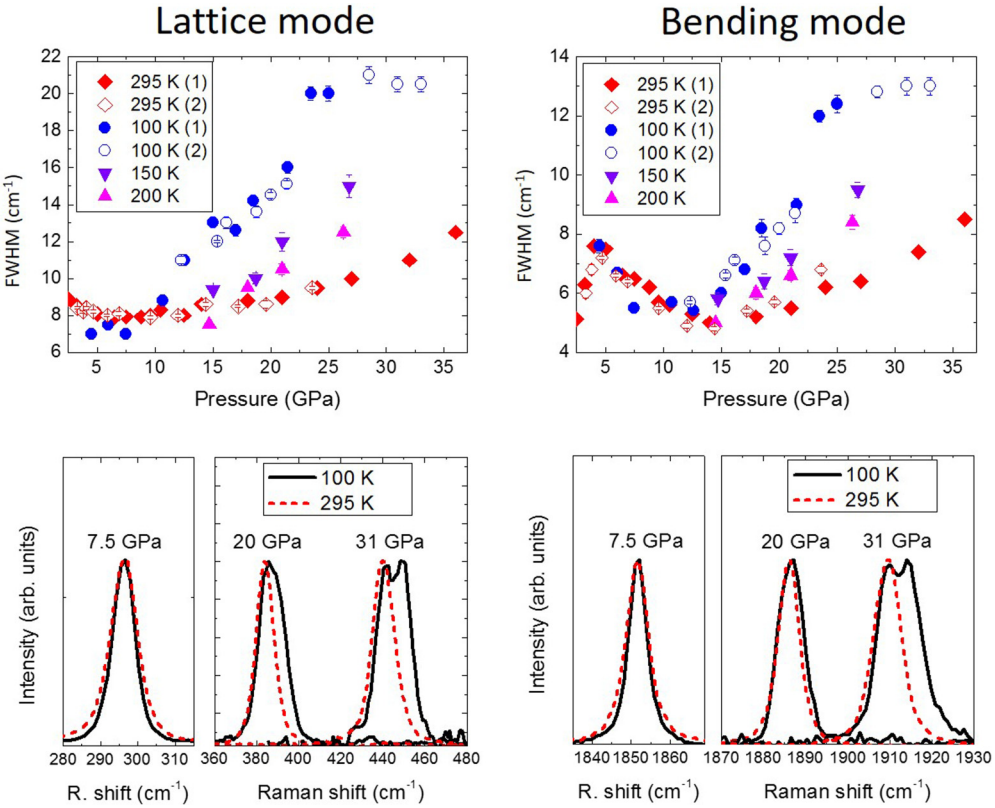

FIG. 6. Top panels: FWHM of the lattice and bending modes as a function of pressure for room temperature, low temperature (100 K), and two intermediate temperatures of 150 and 200 K, and for two different experimental runs labeled (1) and (2). Bottom panels: Experimental Raman spectra for lattice and bending modes. At 7.5 GPa, the line shape at 100 K (black solid line) is expectedly slightly narrower than at 295 K (red dotted line). Above 10 GPa, as pressure increases, the 100 K spectra are significantly broader than the 295 K spectra as a consequence of splitting of the Raman mode in the ordered lower-symmetry NH_4F IIIt phase.

the deviation indicates ordering at ambient temperature above 20 GPa, a point that should be noted for discussion below.

III. HIGH-PRESSURE, LOW-TEMPERATURE RAMAN SPECTROSCOPY

To supplement the results of the x-ray diffraction, which is limited by the large crystal grains in the sample and also by its insensitivity to hydrogen atoms, we resort to high-pressure, low-temperature Raman spectroscopy of NH_4F. A Jobin-Yvon HR-460 single monochromator spectrometer in a backscattering configuration with 1500 grooves/mm grating and equipped with an Andor CCD camera was used. 514.5 nm wavelength radiation from an Ar laser was focused into a 2 μm spot by a long-working-distance Mitutoyo x20 objective. The power of the laser measured directly on the diamond-anvil cell (DAC) was kept below 2 mW to avoid any photoinduced transformation of the sample. Measurements were performed at 295 K between 0.26 and 42 GPa and between 100 and 275 K in steps of 25 K, up to a pressure of 31 GPa.

In Fig. 5, we show Raman spectra of the principal regions for a few chosen pressures. Measurements were made from ambient pressure to 42 GPa and at a temperature of 295 K. NH_4F I, NH_4F II, as well as the cubic NH_4F III phase are all clearly identified by their distinctive Raman spectra. In the three panels, the principal modes are shown, including the transverse-optical (TO) lattice mode (above 200 cm^{-1}) and the internal modes related to bending (above 1400 and 1800 cm^{-1}, respectively, ν_4 and ν_2) and stretching (above 3000 cm^{-1}, ν_3 and ν_1).

Two low-intensity modes are also detected in NH_4F III above 600 cm^{-1} (left panel of Fig. 5) and above 2025 cm^{-1} (middle panel of Fig. 5). The weak feature above 600 cm^{-1} is the librational mode (ν_6) probably observed because the ammonium ion in NH_4F is in a highly asymmetric potential well. In the cubic phases of the other ammonium halides, it is generally detected as a combination mode or an overtone [35]. In NH_4F III, it has been directly observed with inelastic neutron scattering at the wave numbers detected in our experiment [11]. The slightly stronger feature above 2025 cm^{-1} is the ($\nu_4 + \nu_6$) combination mode also observed in the other ammonium halides [34], in particular in ammonium chloride [36]. The pressure dependence of these weak modes, the TO lattice mode, and the ν_2 bending mode are shown in Fig. 6. While the x-ray measurements do not reveal a structural change, all four modes clearly exhibit a change of slope with pressure at about 10 GPa (Fig. 7). Small differences in the pressure corresponding to the change of slope are probably due to the fact that two of the modes are combination modes. In the other ammonium halides, this behavior is an unambiguous signature of a transition from a disordered cubic phase to an ordered cubic phase

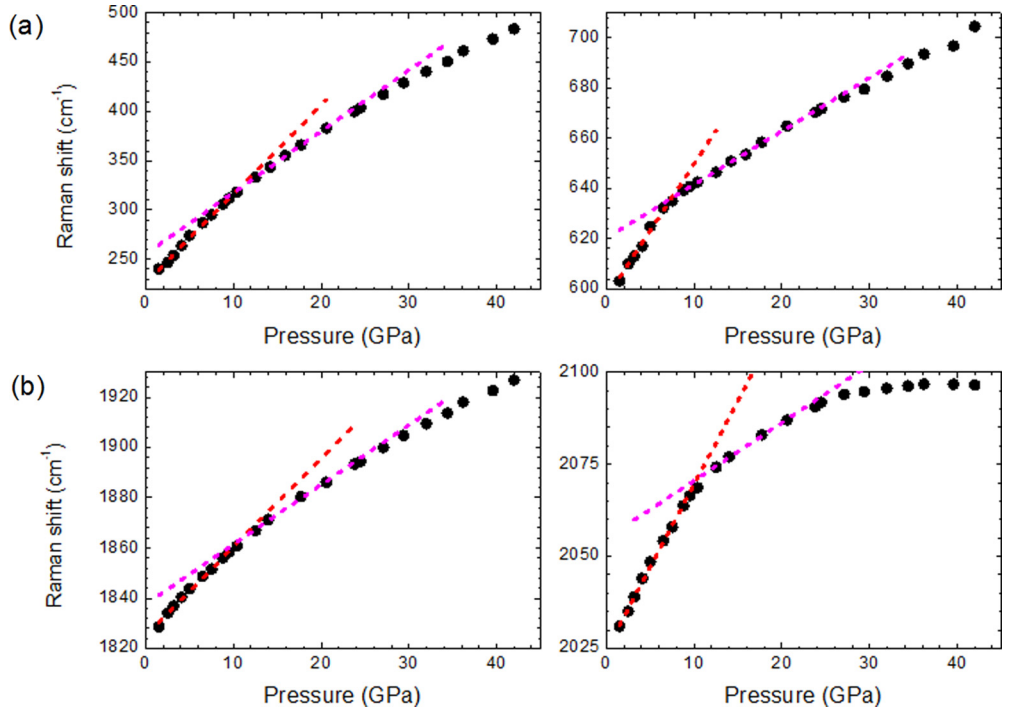

FIG. 7. Variation of the Raman shift as a function of pressure at 295 K for four modes. Linear fits to portions of data highlight a change of slope observed at 10 GPa, signaling the beginning of the disorder-order transition as well as a further change of slope above 20 GPa. (a) The TO lattice mode (left) and the ν_6 librational mode (right). (b) The ν_2 bending mode (left) and the ($\nu_4 + \nu_6$) combination mode (right).

[34,36] with an ordering of the ammonium ion in the crystal structure. Some modes also show a further change of slope at still higher pressure, recalling the anomaly above 20 GPa in the equation of state and indicating a more ordered structure.

We now discuss the line shape and pressure evolution of the stretching modes. The broad stretching band centered around 3000 cm^{-1} observed experimentally is typical of the high-pressure behavior in the N-H stretching region [37,38] or in cubic ice [39], but in contrast with sharper modes measured in the other ammonium halides [31,34,40,41]. On the other hand, in both ice [39,42] and in the halide with the largest ion NH_4I [33], the stretching modes soften with pressure. The reason for this is the increasing strength of hydrogen bonding with pressure which weakens the corresponding covalent bond (H-N or H-O as the case may be) and softens the internal stretching mode. In NH_4F, which is a hydrogen-bonded crystal like ice, the opposite behavior is observed, i.e., the stretching modes harden as in NH_4Cl [40]. This complex trend, combined with the absence of a signature of the order-disorder transition on the stretching modes in some halides [33,34], implies that the behavior of these modes with pressure in NH_4F is not straightforward and may not necessarily reflect changes in hydrogen ordering. We therefore concentrate on the lattice and bending modes in the following.

The disorder-order transitions in the cubic phases of the other ammonium halides as well as in ice also depend on temperature. Notably, disordered cubic ice VII transforms to ordered tetragonal ice VIII. Two recent reports [43,44] indicate that this transition is accompanied by a splitting of the principal lattice mode at high pressure in ice VIII. To investigate this aspect, we make temperature-dependent Raman measurements with regular steps from 295 to 100 K for several pressures from 2 to 35 GPa, and in two different runs to test repeatability. At low pressures, line shapes are slightly narrower at low temperatures, as expected due to increase in the phonon lifetime. A progressive and marked change occurs in the bending and the lattice modes [Fig. 6(a)] above 10 GPa. The principal Raman line in each of these regions begins to broaden as temperature is decreased from 295 to 100 K. The broadening increases *and* is detected at higher temperatures as pressure increases. At 100 K and beyond 20 GPa, the broadening undergoes a jump and stabilizes with a visible splitting of the main lines.

IV. DISCUSSION

The broadening and splitting of the bending and lattice modes in going from 295 to 100 K above 10 GPa are compatible with a subtle lowering of symmetry. The dependence on temperature rules out an extrinsic effect related to nonhydrostatic conditions, which are also precluded by our use of a neon pressure medium. The other ammonium halides [15,16] and ice [45] are known to undergo temperature-dependent order-disorder transitions related to the hydrogen bond, though no such transition has been reported in NH_4F. In NH_4Cl [31], NH_4Br [32], and in NH_4I [33], this transition to the ordered phase is accompanied by a splitting of the lattice mode which accentuates with pressure. However, these earlier works have not dwelt on the reasons for this splitting or its mechanism as the temperature is lowered. Here we give an explanation based on both our measured Raman spectra and our simulations. The observed splitting of the lattice and bending modes cannot

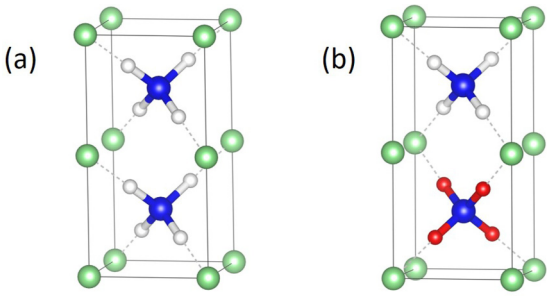

FIG. 8. Small spheres (gray) represent hydrogen, the central sphere (blue) represents nitrogen, and corner spheres (green) represent fluorine. (a) The tetragonal $P\bar{4}2m$ structure, which is the ordered low-temperature phase. (b) The tetragonal $P4_2/mcm$ structure.

result just from the ordering transition. The calculated spectra for the ordered $P\bar{4}3m$ structure are unequivocally single mode in both of these regions. Besides, no other lower-symmetry structure is found in these regions apart from the ordered $P\bar{4}3m$ structure. The splitting of the modes can only be due to a lowering of symmetry. We look for the simplest explanation, which is a small spontaneous tetragonal distortion of the cubic CsCl structure at low temperature. We will label this low-temperature phase NH_4F IIIt. Our simulations (see Supplemental Material [23]) also show Raman mode splitting in the tetragonal structure with the $P\bar{4}2m$ space group.

Both Raman and x-ray diffraction indicate a disordered high-temperature $P\bar{4}3m$ NH_4F III cubic phase which undergoes ordering above 10 GPa. Disorder-order transitions are also found in the other ammonium halides. The splitting of the Raman lattice and bending modes at low temperature also indicates a transition towards a tetragonally distorted NH_4F IIIt phase for pressures higher than 10 GPa. As pressure increases, this transition shifts towards higher temperatures and appears to be complete above 20 GPa. Is ordering compatible with a tetragonal distortion? To clarify this point, we have calculated the thermodynamic cost of the above tetragonal distortion for two cubic $P\bar{4}3m$ unit cells stacked along the c axis. The first stack shown in Fig. 8(a) is of identical $P\bar{4}3m$ unit cells, giving rise to the $P\bar{4}2m$ structure on distortion. The second stack shown in Fig. 8(b) is of two $P\bar{4}3m$ cells but with a 90° rotation of the NH_4^+ tetrahedron around the c axis between the two cells, representing rotational disorder as in our $2 \times 2 \times 2$ supercell, and giving rise to a $P4_2/mcm$ unit cell on distortion. While the enthalpies of the $P\bar{4}3m$ and $P\bar{4}2m$ structures are within a few meV/f.u. over the entire pressure range, the enthalpy of the $P4_2/mcm$ structure is more than 50 meV/f.u. higher. This indicates that the low-temperature ordered, tetragonally distorted phase is energetically favored. Again, simulated Raman spectra for the $P\bar{4}2m$ structure are in much better agreement (see Supplemental Material [23]) with our experimental data than those for the $P4_2/mcm$ structure.

V. CONCLUSION

In conclusion, using high-pressure x-ray diffraction, high-pressure and low-temperature Raman spectroscopy, and *ab initio* structure search calculations, we have found an ordered low-temperature phase, NH_4F IIIt, and an accompanying disorder-order transition from the cubic NH_4F III phase. NH_4F is simultaneously an ammonium halide and an icelike molecular crystal bound with hydrogen bonds, an ambiguity reflected in our results. On the one hand, we detect a disorder-order transition in NH_4F III similar to the one found in the other ammonium halides. This transition sets in above 10 GPa and is detected in the pressure dependence of several Raman modes. On the other hand, as pointed out earlier, all three phases of NH_4F closely resemble those found in ice in a similar pressure range. Moreover, at low temperatures, we find a subtle distortion from cubic NH_4F III to slightly tetragonal NH_4F IIIt. This disorder-order transition thus also bears a similarity to the cubic-tetragonal, ice VII–ice VIII disorder-order transition.

ACKNOWLEDGMENTS

A.M. and A.M.S. acknowledge the GENCI IDRIS and CINES French national supercomputing facilities for CPU time (Project No. 2015-091387). C.N. thanks the Université Pierre and Marie Curie for hosting him. We thank Livia Bove (IMPMC) for a critical reading of the manuscript.

[1] S. L. Mair, Acta Crystallogr. Sect. A **34**, 656 (1978).
[2] R. J. C. Brown, J. Mol. Struct. **345**, 77 (1995).
[3] B. Barbiellini, C. Bellin, G. Loupias, T. Buslaps, and A. Shukla, Phys. Rev. B **79**, 155115 (2009).
[4] W. Zachariasen, Z. Phys. Chem. **127**, 218 (1927).
[5] H. W. W. Adrian and D. Feil, Acta Crystallogr. Sect. A **25**, 438 (1969).
[6] M. A. Nabar, L. D. Calvert, and E. Whalley, J. Chem. Phys. **51**, 1353 (1969).
[7] A. C. Lawson, R. B. Roof, J. D. Jorgensen, B. Morosin, and J. E. Schirber, Acta. Crystallogr. Sec. B **45**, 212 (1989).
[8] A. K. Kuriakose and E. Whalley, J. Chem. Phys. **48**, 2025 (1968).
[9] C. W. F. T. Pistorius, J. Chem. Phys. **50**, 1436 (1969).
[10] K. W. Suh, K.-J. Oh, S.-J. Jeon, and D.-H. Kim, Bull. Korean Chem. Soc. **13**, 575 (1992).
[11] V. P. Glazkov, D. P. Kozlenko, B. N. Savenko *et al.*, Crystallogr. Rep. **44**, 50 (1999).
[12] W. B. Kamb, Acta Crystallogr. **17**, 1437 (1964).
[13] J. D. Jorgensen and T. G. Worlton, J. Chem. Phys. **83**, 329 (1985).
[14] J. M. Besson, P. Pruzan, S. Klotz, G. Hamel, B. Silvi, R. J. Nelmes, J. S. Loveday, R. M. Wilson, and S. Hull, Phys. Rev. B **49**, 12540 (1994).
[15] N. G. Parsonage and L. A. K. Staveley, *Disorder in Crystals* (Clarendon, Oxford, 1978).
[16] R. G. Ross and P. Andersson, J. Phys. C **20**, 4745 (1987).
[17] J. C. Chervin, B. Canny, and M. Mancinelli, High Press. Res. **21**, 305 (2002).
[18] A. Hammersley, S. Stevenson, M. Hanfland, A. Fitch, and D. HÃusermann, High Press. Res. **14**, 235 (1996).
[19] H. M. Rietveld, J. Appl. Crystallogr. **2**, 65 (1969).

[20] J. Rodriguez-Carvajal, Physica B (Amsterdam) **192**, 55 (1993).
[21] F. D. Murnaghan, Proc. Natl. Acad. Sci. USA **30**, 244 (1944).
[22] C. J. Pickard and R. J. Needs, J. Phys.: Condens. Matter **23**, 053201 (2011).
[23] See Supplemental Material at http://link.aps.org/supplemental/10.1103/PhysRevB.96.094110 for details of the calculations, which includes Refs. [24-27].
[24] S. J. Clark, M. D. Segall, C. J. Pickard, P. J. Hasnip, M. I. J. Probert, K. Refson, and M. C. Payne, Z. Kristallogr. **220**, 567 (2005).
[25] D. Vanderbilt, Phys. Rev. B **41**, 7892 (1990).
[26] H. J. Monkhorst and J. D. Pack, Phys. Rev. B **13**, 5188 (1976).
[27] S. Baroni, S. de Gironcoli, A. D. Corso, and P. Giannozzi, Rev. Mod. Phys. **73**, 515 (2001).
[28] P. Giannozzi *et al.*, J. Phys.: Condens. Matter **21**, 395502 (2009).
[29] J. P. Perdew, K. Burke, and M. Ernzerhof, Phys. Rev. Lett. **77**, 3865 (1996).
[30] J. P. Perdew, A. Ruzsinszky, G. I. Csonka, O. A. Vydrov, G. E. Scuseria, L. A. Constantin, X. Zhou, and K. Burke, Phys. Rev. Lett. **100**, 136406 (2008).
[31] M. Couzi, J. B. Sokoloff, and C. H. Perry, J. Chem. Phys. **58**, 2965 (1973).
[32] H. D. Hochheimer and T. Geisel, J. Chem. Phys. **64**, 1586 (1976).
[33] A. M. Heyns, K. R. Hirsch, and W. B. Holzapfel, J. Chem. Phys. **73**, 105 (1980).
[34] Y. Ebisuzaki, Chem. Phys. Lett. **19**, 503 (1973).
[35] Y. Ebisuzaki, J. Chem. Phys. **61**, 3170 (1974).
[36] Y. Ebisuzaki and M. Nicol, Chem. Phys. Lett. **3**, 480 (1969).
[37] C. J. Pickard and R. J. Needs, Nat. Mater. **7**, 775 (2008).
[38] S. Ninet, F. Datchi, P. Dumas, M. Mezouar, G. Garbarino, A. Mafety, C. J. Pickard, R. J. Needs, and A. M. Saitta, Phys. Rev. B **89**, 174103 (2014).
[39] C.-S. Zha, J. S. Tse, and W. Bassett, J. Chem. Phys. **145**, 124315 (2016).
[40] A. M. Heyns, J. Phys. Chem. Solids. **41**, 769 (1979).
[41] L. R. Fredrickson and J. C. Decius, J. Chem. Phys. **66**, 2297 (1977).
[42] P. Pruzan, J. C. Chervin and M. Gauthier, Europhys. Lett. **13**, 81 (1990).
[43] Ph. Pruzan, J. C. Chervin, E. Wolanin, B. Canny, M. Gauthier, and M. Hanfland, J. Raman Spectrosc. **34**, 591 (2003).
[44] Y. Yoshimura, S. T. Stewart, M. Somayazulu, H.-k. Mao, and R. J. Hemley, J. Chem. Phys. **124**, 024502 (2006).
[45] V. F. Perenko and R. W. Whitworth, *Physics of Ice* (Oxford University Press, New Yrok, 1999).